Available online at www.sciencedirect.com
SCIENCE DIRECT®
ELSEVIER
International Journal of Solids and Structures 43 (2006) 2932–2958
INTERNATIONAL JOURNAL OF SOLIDS and STRUCTURES
www.elsevier.com/locate/ijsolstr

Some recent developments on integrity assessment of pipes and elbows. Part II: Experimental investigations

J. Chattopadhyay [a,*], H.S. Kushwaha [a], E. Roos [b]

[a] *Reactor Safety Division, Hall-7, Bhabha Atomic Research Centre, Mumbai 400085, India*
[b] *Material Testing Institute, MPA, Pfaffenwaldring 32, University of Stuttgart, D-70569 Stuttgart, Germany*

Received 28 January 2005; received in revised form 13 June 2005
Available online 18 August 2005

Abstract

Integrity assessment of piping components is very essential for safe and reliable operation of power plants. Over the last several decades, considerable work has been done throughout the world to develop a methodology for integrity assessment of pipes and elbows, appropriate for the material involved. However, there are scope of further development/improvement of issues, particularly for pipe bends, that are important for accurate integrity assessment of piping. Considering this aspect, a comprehensive *Component Integrity Test Program* was initiated in 1998 at Reactor Safety Division (RSD) of Bhabha Atomic Research Centre (BARC), India in collaboration with MPA, Stuttgart, Germany through Indo-German bilateral project. In this program, both theoretical and experimental investigations were undertaken to address various issues related to the integrity assessment of pipes and elbows. The important results of the program are presented in this two-part paper. In the part II of the paper, the experimental investigations are discussed. Part I covered the theoretical investigations. Under the experimental investigations, fracture mechanics tests have been conducted on pipes and elbows of 200–400 mm diameter with various crack configurations and sizes under different loading conditions. Tests on small tensile and three point bend specimens, machined from the tested pipes, have also been done to evaluate the actual stress–strain and fracture resistance properties of pipe/elbow material. The load–deflection curve and crack initiation loads predicted by non-linear finite element analysis matched well with the experimental results. The theoretical collapse moments of throughwall circumferentially cracked elbows, predicted by the recently developed equations, are found to be closer to the test data compared to the other existing equations. The role of stress triaxialities ahead of crack tip is also shown in the transferability of *J*–resistance curve from specimen to component.

Keywords: Pipe; Pipe bend; Crack; Integrity assessment; Limit load; Fracture experiment

* Corresponding author. Tel.: +91 22 25591522; fax: +91 22 25505151.
E-mail address: jchatt@apsara.barc.ernet.in (J. Chattopadhyay).

0020-7683/$ - see front matter © 2005 Elsevier Ltd. All rights reserved.
doi:10.1016/j.ijsolstr.2005.06.055

Nomenclature

a	crack length per crack tip
A_{nq}	modified triaxiality parameter (Eq. (18))
D, D_m, D_N	outer, mean, nominal diameter of pipe/elbow cross section
E	Young's modulus
h	$= tR_b/R^2$, elbow factor or pipe bend characteristics
J	J-integral
$(J_i)_{SZW}$	J-initiation toughness from stretched zone width
M	total applied moment
M_L	limit moment (collectively used to define instability or collapse moment)
M_0	limit moment (collectively used to indicate instability or collapse) for defect-free pipe/elbow
P	total applied load
q	triaxiality parameter (Eq. (15))
R	mean radius of pipe/elbow cross section
R_b	bend radius of elbow at crown
t	wall thickness of pipe/elbow
t_{av}	average wall thickness of elbow in crack section
X	$= M_L/M_0$, weakening factor of throughwall circumferentially cracked elbow collapse moment due to the presence of crack

Greek symbols

θ	half circumferential crack angle
σ_y	material yield stress
σ_f	material flow stress defined as the average of yield and ultimate strength

Abbreviations

CMOD	crack mouth opening displacement
COD	crack opening displacement
J–R	J–resistance
J–T	J-integral–tearing modulus
NB	nominal bore diameter
TCC	throughwall circumferentially cracked
TPB	three point bend

1. Introduction

Integrity assessment of piping components is very essential for safe and reliable operation of both conventional and nuclear power plants. It is especially important for nuclear power plants because of the application of leak-before-break (LBB) concept, which involves detailed integrity assessment of primary heat transport system piping with postulated cracks. The mechanical evaluation of pipe failures has evolved over time. While a considerable work has already been done in the last few decades to develop integrity assessment procedure of cracked/un-cracked piping components, some issues are still unresolved or not fully resolved, especially regarding elbows.

To address these issues, a comprehensive *Component Integrity Test Program* was initiated in 1998 at Bhabha Atomic Research Centre (BARC), India in collaboration with MPA, Stuttgart, Germany. In this program, both theoretical and experimental investigations were undertaken to address various issues related to the integrity assessment of pipes and elbows. The important results of the program are presented in this two-part paper. Part I of the paper (Chattopadhyay et al., 2005b) covered the theoretical study. In this Part II, the experimental investigations are described.

In the experimental investigations, fracture mechanics tests are carried out on cracked pipes and elbows under quasi-static monotonic loading to validate some of the new theoretical development mentioned in Chattopadhyay et al. (2005b) and also to address the issue of transferability of fracture data from specimen to component. Total 45 tests consisting of 27 pipes of various sizes (200–400 mm diameter) with circumferential cracks of various angles (30–150°), configurations (throughwall/surface), materials (base/weld) and 18 elbows of various sizes (200–400 mm diameter) with throughwall cracks of various angles (60–120°), locations (extrados/intrados/crown), configurations (circumferential/axial) and in-plane bending modes (opening/closing) have been tested. However, out of all of them, test results of 7 pipes and 10 elbows are reported here. Tests on small tensile and SE(B) (also known as three point bend, TPB) specimens, machined from the pipe of same material and heat, have also been done to evaluate the actual stress–strain and fracture resistance properties of pipe/elbow material. Finally numerical and analytical studies are performed on these tested specimens and components to compare the test results with the theoretical predictions and also to study the role of stress triaxialities in the transferability of J–resistance curve from specimen to component.

2. Fracture tests on straight pipes

2.1. Test specimens

Test specimens consist of straight pipes made of SA333 Gr6 carbon steel material with throughwall circumferential crack at the middle of its length. Fig. 1 shows the geometry of the pipe specimens. These pipe specimens are subjected to four point bending load. The notched test specimens are fatigue pre-cracked by small amount (~2–10 mm at each side) prior to performing the experiment. This ensures a sharp crack tip. During the fatigue pre-crack, sinusoidal cyclic load is applied. The maximum cyclic load is approximately 10% of the collapse load and minimum cyclic load is 10% of the maximum load. The geometric details of the test specimens are given in Table 1.

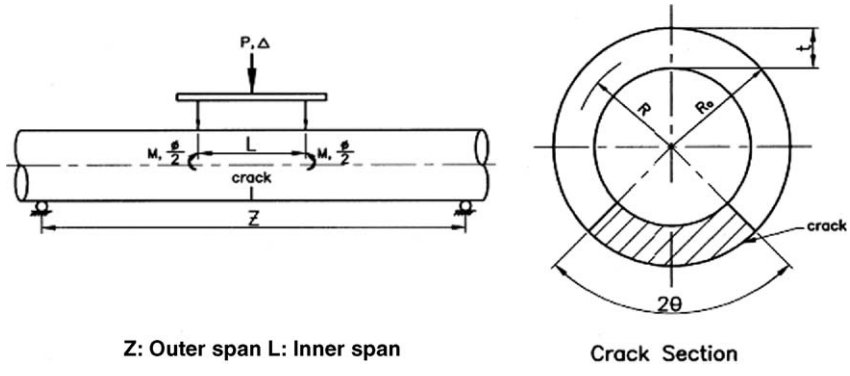

Fig. 1. Pipe with throughwall circumferential crack under four point bending load.

Table 1
Details of pipe test specimens

Test no.	Outer dia. (mm)	Thickness (mm)	Outer span (Fig. 1) (mm)	Inner span (Fig. 1) (mm)	Crack angle, $2\theta°$	
					As machined	After fatigue pre-crack
SP BM TWC8-1[a]	219	15.15	4000	1480	60.0	65.6
SP BM TWC8-2	219	15.10	4000	1480	90.0	93.9
SP BM TWC8-3	219	15.29	4000	1480	120.0	126.4
SP BM TWC8-4	219	15.11	4000	1480	150.0	157.0
SP BM TWC16-1	406	32.38	5820	1480	90.9	96.0
SP BM TWC16-2	406	32.15	5820	1480	121.4	126.3
SP BM TWC16-3	406	32.36	5820	1480	153.0	157.8

[a] SP = straight pipe, BM = base metal, TWC = throughwall crack, first number represent the nominal pipe diameter in inch and second number represents the test number.

2.2. Test arrangement

Tests are carried out on the fatigue pre-cracked pipe specimens at room temperature. Similar type of tests on pipes and its analysis had been reported by several researchers e.g. Moulin and Delliou (1996), Kashima et al. (1990), Wilkowski et al. (1989), Roos et al. (2000), Darlaston et al. (1992) and Forster et al. (1996). In the present work, tests are conducted on carbon steel pipes under four point bend loading using computer controlled servo-hydraulic actuator of ± 1 MN capacity. Fig. 2 shows the test set-up. The outer span of four point bend loading has been 4 and 5.82 m in case of 200 and 400 mm NB pipes respectively. The inner span of loading is 1.48 m. Static (monotonic) load is applied on the pipe specimens under displacement control. The rate of displacement has been fixed as 0.055 mm/s.

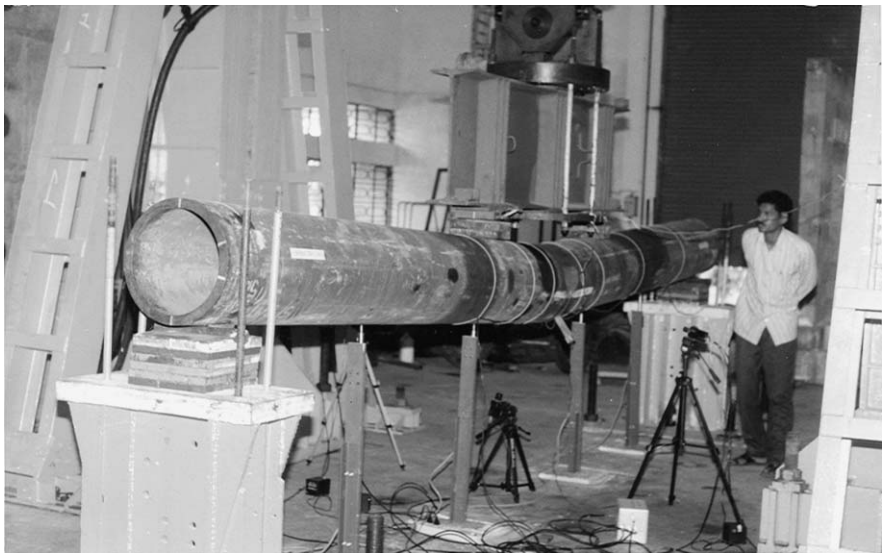

Fig. 2. Photograph of pipe fracture test set-up.

2.3. Instrumentation and data acquisition

During the fracture experiments, instrumentation are mounted to measure the various parameters, namely, total applied load, load line displacement, crack growth at both the crack tips, crack opening displacement at various locations of the notch, deflection of pipe at typical locations.

The total applied load is measured directly using a strain gauge based load cell connected to the actuator. The load-line displacement is measured by an in-built linear variable displacement transducer (LVDT) of the actuator.

Crack growth is measured by image processing system. Crack opening displacements at crack mouth and at various locations along the length of the crack are measured by clip gauges and image processing technique. The deflections of pipe at some selected locations are measured by LVDT. More details of the test arrangement and image processing system are described in Chattopadhyay et al. (2000) and Joshi et al. (1999).

2.4. Test results of cracked pipes

Pipe test results are obtained in the form of load vs. load-point deflection, crack growth and crack opening displacement curves. Fig. 3 shows the load vs. load-point deflection curves for various pipes. Crack grows out-of-plane in case of carbon steel pipes. The amount of crack growth is slightly different at two crack tips. To construct the load vs. crack growth (in circumferential direction) curves and generate the component J–R curves, the average projected crack growth in the plane of the initial crack is taken. Fig. 4 shows the load vs. crack growth curves for various pipes. Fig. 5 shows the photograph of the typical crack growth in one of the pipes. Fig. 6 shows the images of complete crack growth process at one tip of the crack for fracture test no. SPBMTWC8-3. It shows first the blunting of the sharp crack tip that is generated during fatigue pre-crack, its out-of-plane crack growth and taking turn following a zig-zag path.

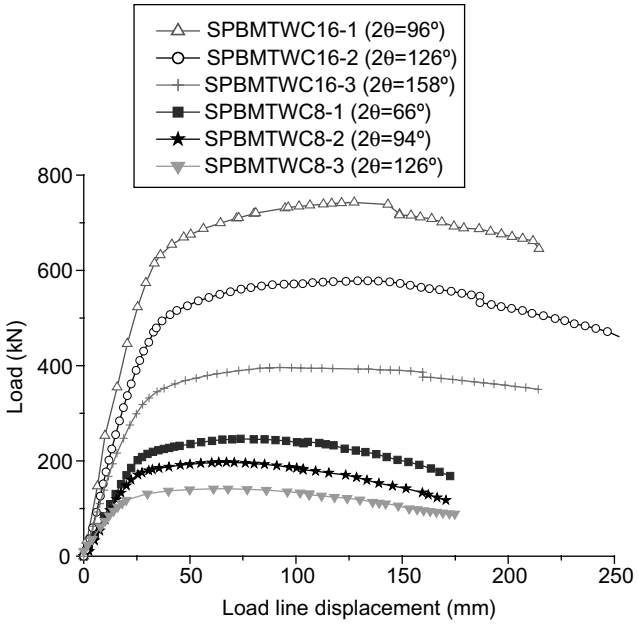

Fig. 3. Load vs. load-line-displacement curves for various pipes.

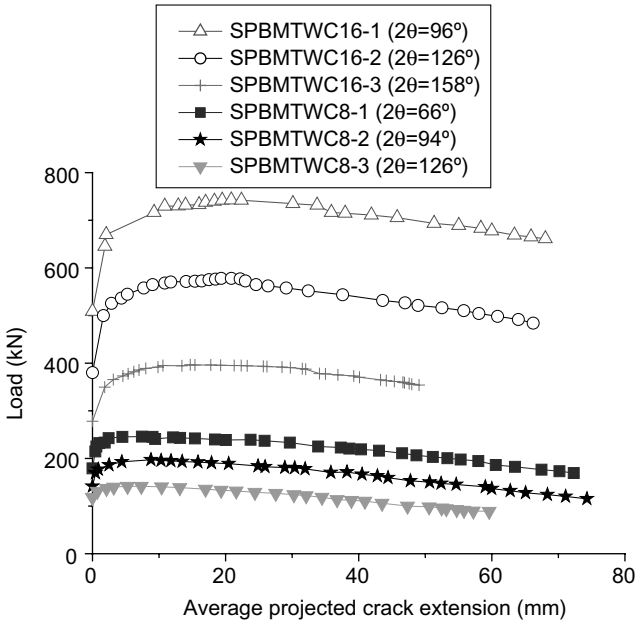

Fig. 4. Load vs. crack growth curves for various pipes.

Fig. 5. Typical crack growth pattern in pipe test specimen no. SPBMTWC8-1.

3. Fracture tests on elbow

Test data on cracked elbows are not so abundant as straight pipes. Experiments were carried out on elbows by Greenstreet (1978), Griffiths (1979), Moulin et al. (1989) and Yahiaoui et al. (2000, 2002). These

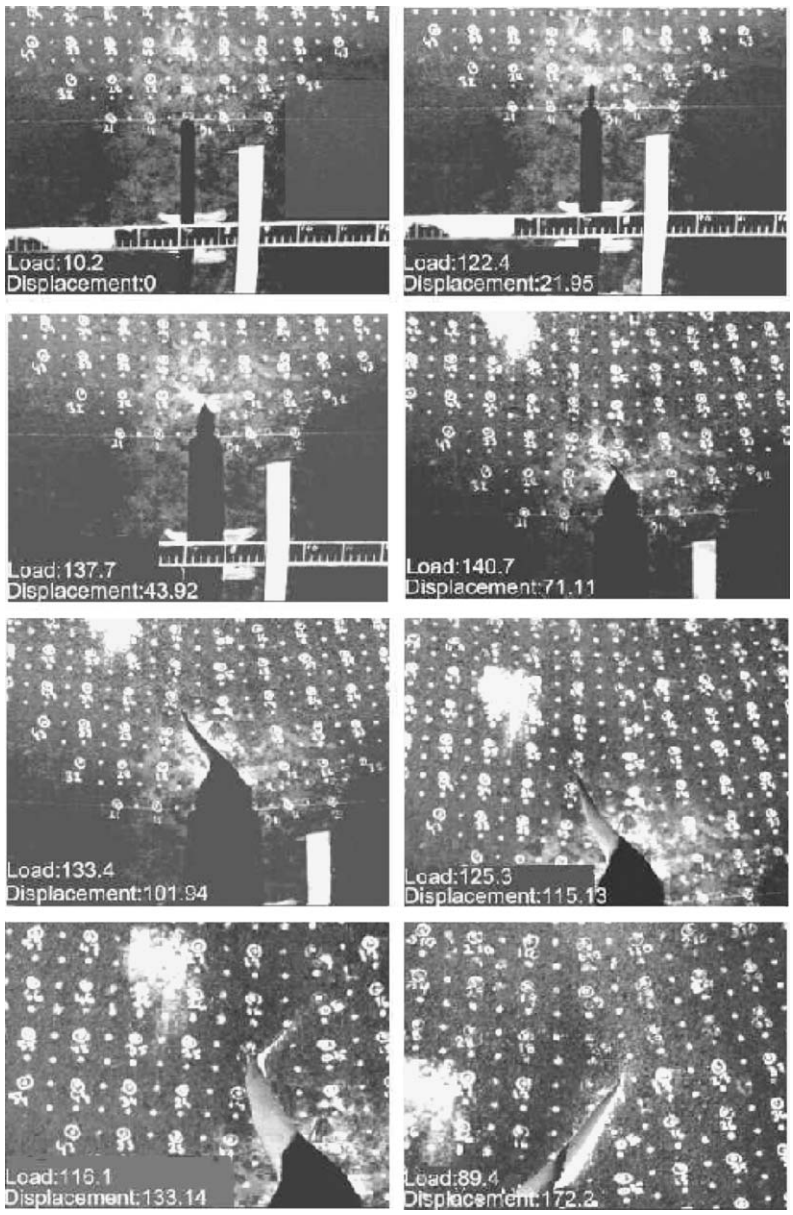

Fig. 6. Crack growth images at various stages of loading in carbon steel pipe test no. SPBMTWC8-3 (load in kN and displacement in mm).

experiments covered elbows without defect and with throughwall axial/circumferential and part-through cracks. Under the second part of the International Piping Integrity Group (IPIRG-2) Program (Wilkowski et al., 1998), few experiments were also carried out on elbows. However, the thrust of all the above-mentioned experiments was mainly the evaluation of limit load from load–deflection data. No data on the measurement of fracture parameters e.g. crack growth, crack initiation loads or crack opening displacement (COD) were reported in these papers. Considering this aspect of the earlier experiments and also the need

to have abundant fracture test data of throughwall cracked elbows for validation of new developments in theoretical aspect of integrity assessment of elbows, fracture tests have been carried out on throughwall cracked carbon steel elbows of 200–400 mm nominal bore (NB) diameter. The present set of experiments are carried out at room temperature on 18 carbon steel elbows with throughwall circumferential/axial cracks subjected to in-plane bending moments. Out of 18 elbows, 10 cases are reported in this paper. These test data have been analyzed numerically through non-linear finite element analyses, analytically through limit load comparison and also through comparison of crack initiation loads. The following paragraphs describe various aspects of these experiments. More details of these tests may be available in Chattopadhyay et al. (2005a).

3.1. Test specimens and set-up

Test specimens consist of four 200 mm and six 400 mm nominal bore (NB) diameter 90° elbows made of ASTM-A333 Gr.6 carbon steel material having a throughwall crack. Three crack configurations are tested—throughwall circumferential crack at extrados subjected to closing moment (Fig. 7), throughwall circumferential crack at intrados subjected to opening moment (Fig. 8) and throughwall axial crack at elbow crown subjected to closing and opening moments (Fig. 9). The thickness of elbows along the circumference of the cracked section varies due to the forming process. For each elbow, the thickness has been measured at 24 locations along the circumference of the crack plane and an average value is taken for the calculations. The straight pipes of length of 600 mm are welded on both sides of the 200 mm NB elbow. The length of straight pipe is 400 mm in case of 400 mm NB elbows. The reason for shorter length of straight pipe for 400 mm NB elbows is the limitation of the test set-up to accommodate maximum 3 m height of the test specimen. The other end of the straight pipe is welded to a 900 lbs. 200 or 400 mm NB flange, which is bolted to a circular plate. Fig. 10 shows the schematic drawing of test set-up.

Out of 10 elbows tested, four have throughwall circumferential cracks at the intrados and are subjected to opening bending moment, four have throughwall circumferential cracks at the extrados and are subjected to closing bending moment and two have throughwall axial cracks at the crown. Out of two axially cracked elbows, one (200 mm NB) is subjected to closing moment and another (400 mm NB) is subjected to opening moment. Cracks have been machined on the elbows by a milling process. Before carrying out the fracture tests, each elbow is fatigue pre-cracked through remote loading by around 3–10 mm on each side of the crack to have sharp crack tips. It was periodically checked by non-corrosive dye penetrant.

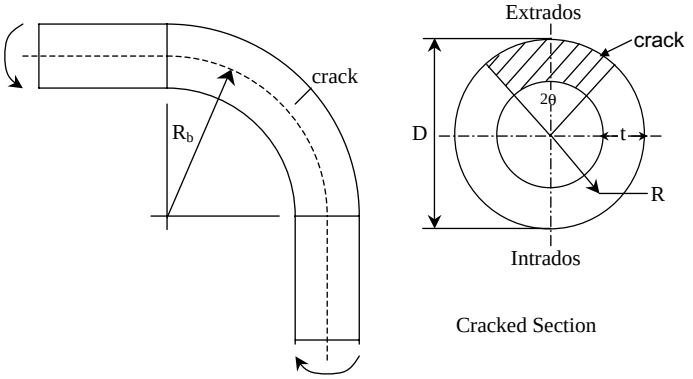

Fig. 7. Schematic drawing of elbow test specimen with throughwall circumferential crack at extrados subjected to closing bending moment.

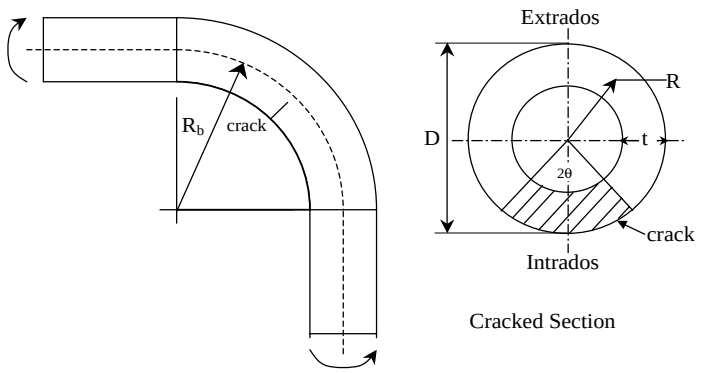

Fig. 8. Schematic drawing of elbow with throughwall circumferential crack at intrados subjected to opening bending moment.

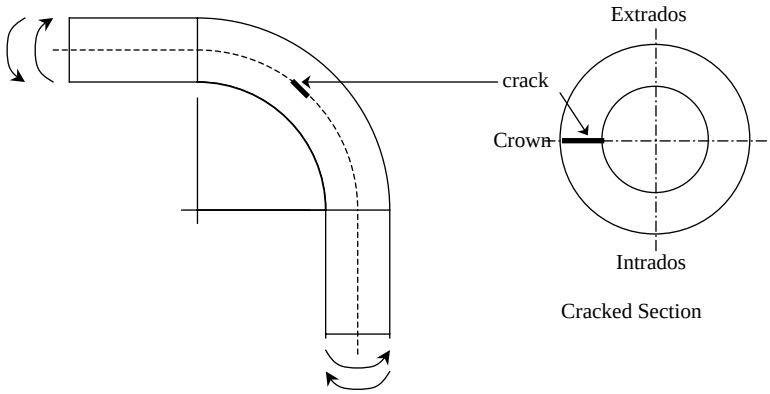

Fig. 9. Schematic drawing of elbow with throughwall axial crack at crown subjected to closing/opening bending moment.

These fatigue pre-cracked elbows are then subjected to in-plane opening/closing bending moment in a quasi-static manner as shown in Fig. 10. Table 2 shows the geometric details of the elbows. The moment at elbow mid-section is obtained by multiplying the load with the perpendicular distance between the load line and mid-section of elbow centerline. These distances are 825.72 and 840.22 mm for 200 and 400 mm NB elbows respectively. Although these distances change during loading of the elbow, the change is negligible compared to the initial distance and hence not considered in the calculation. Fig. 11 shows the photograph of one typical 200 mm NB elbow test rig. Crack growth is measured by image processing technique (Chattopadhyay et al., 2000; Joshi et al., 1999). At the end of test, the fatigue pre-crack length has been precisely measured after breaking open the crack surface. Crack mouth opening displacement (CMOD) is measured by clip gauge mounted on two knife edges, spot-welded at the middle of crack length.

3.2. Experimental results

Load–deflection curve for each elbow specimen has been obtained. From these load–deflection curves, collapse loads are evaluated by twice-elastic slope (TES) method. Figs. 12 and 13 show the experimental load–deflection curves for 200 and 400 mm NB elbows respectively. The TES collapse points are also shown in these figures. Experiment on axially cracked 400 mm NB elbow (test no. ELTWCR16-6) were discontinued before attainment of maximum load because the load went beyond the maximum capacity of the

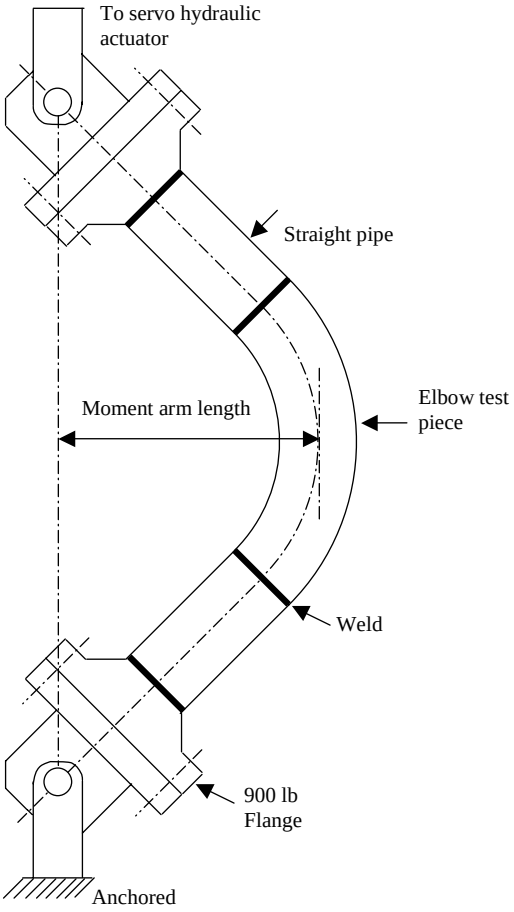

Fig. 10. Schematic drawing of elbow test set-up.

Table 2
Details of elbow test specimens

Test reference number	R_b (mm)	D (mm)	t_{av} (mm)	Moment arm length[a] (Fig. 10) (mm)	Crack orientation	Crack location	Bending mode	Crack angles after fatigue pre-crack (2θ)
ELTWIN8-1	207	219	19.1	825.72	Circumferential	Intrados	Opening	94.96°
ELTWIN8-2	207	219	18.8	825.72	Circumferential	Intrados	Opening	125.16°
ELTWEX8-4	207	219	19.3	825.72	Circumferential	Extrados	Closing	98.24°
ELTWEX8-6	207	219	19.0	825.72	Axial	Crown	Closing	$2a = 109.2$ mm
ELTWIN16-1	609	406	36.4	840.22	Circumferential	Intrados	Opening	95.89°
ELTWIN16-2	609	406	36.8	840.22	Circumferential	Intrados	Opening	122.79°
ELTWEX16-3	609	406	35.1	840.22	Circumferential	Extrados	Closing	64.85°
ELTWEX16-4	609	406	35.7	840.22	Circumferential	Extrados	Closing	94.11°
ELTWEX16-5	609	406	37.6	840.22	Circumferential	Extrados	Closing	124.0°
ELTWCR16-6	609	406	36.2	840.22	Axial	Crown	Opening	$2a = 210$ mm

[a] Moment arm length is the perpendicular distance between the loading line and mid-section of elbow center-line for conversion of load to moment.

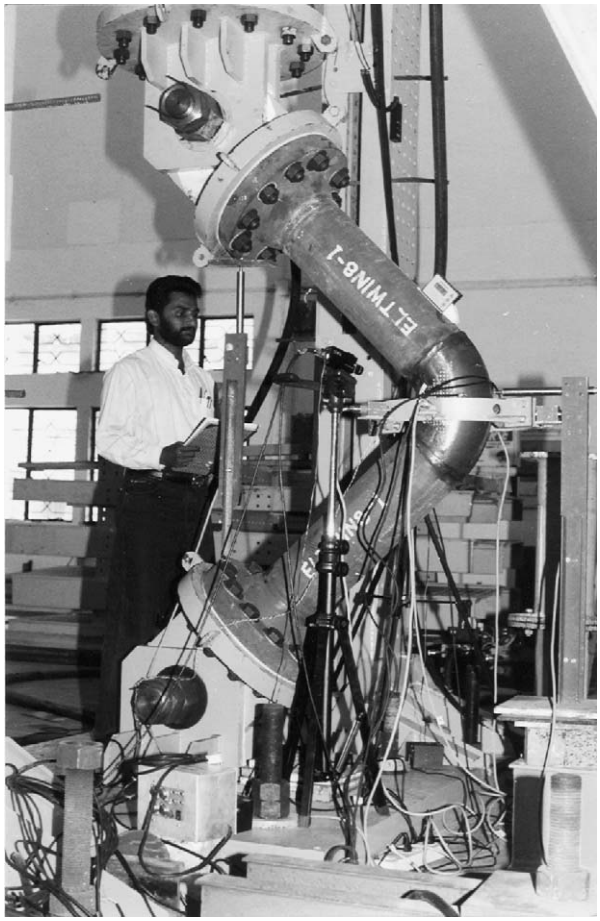

Fig. 11. Photograph of elbow test set-up.

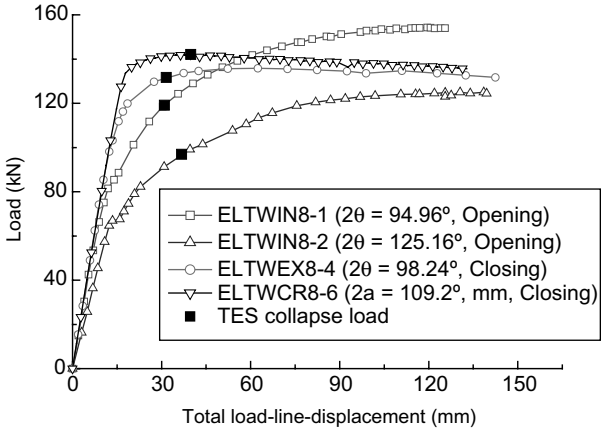

Fig. 12. Experimental load–deflection curves from 200 mm NB elbows.

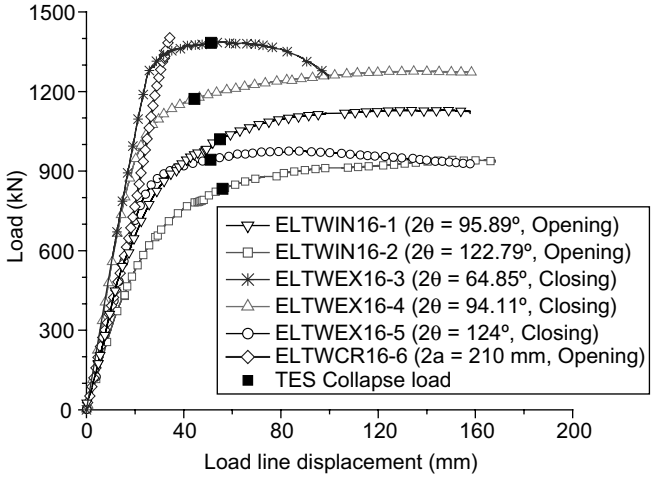

Fig. 13. Experimental load–deflection curves from 400 mm NB elbows.

fixture. Few points may be noted from these load–deflection curves. Firstly, for the same bending mode (i.e. opening/closing), an elbow with higher circumferential crack angle shows lower stiffness and load bearing capacity. This is quite natural as higher crack size weakens an elbow to a greater extent, which reduces its stiffness and load bearing capacity.

Secondly, an elbow with a certain size of throughwall circumferential crack subjected to opening mode of bending moment has lower collapse load compared to an elbow with the same size of crack subjected to closing moment. The same behavior has been observed in the numerical analysis, which is described in detail in Chattopadhyay et al. (2004a,b).

Thirdly, an elbow when tested under displacement controlled set-up and subjected to closing bending moment, load starts falling after certain displacement. In contrast, an elbow when subjected to opening

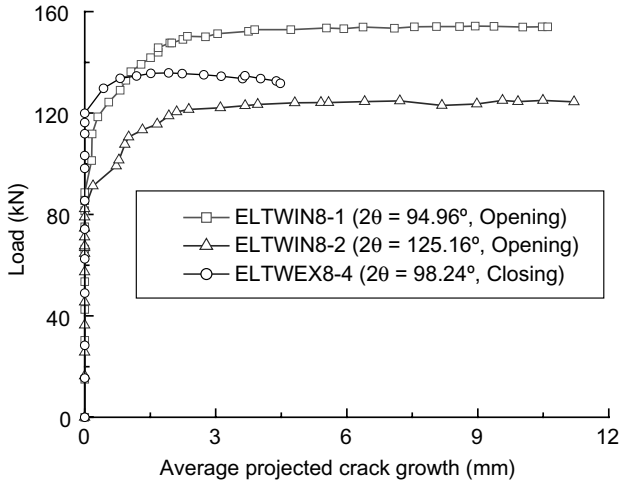

Fig. 14. Experimental load–crack growth curves from 200 mm NB elbows.

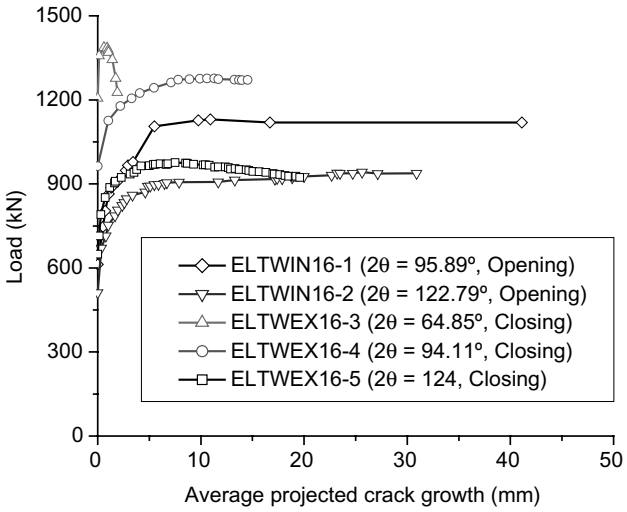

Fig. 15. Experimental load–crack growth curves from 400 mm NB elbows.

bending moment, load does not fall even at large displacement. The reason for this behavior has been explained in Chattopadhyay et al. (2005a) and is not repeated here.

Figs. 14 and 15 show the crack growth observed on outer surface during experiments for 200 and 400 mm NB elbows respectively. Axially cracked elbows with $a/D_m \approx 0.28$ behaved almost like a defect-free elbow, as there was no crack initiation. This is because, at crown (also called flank) of the elbow subjected to in-plane bending moment, hoop stress which is responsible for opening an axial crack is compressive across half of the thickness and hence cannot open a throughwall crack. Figs. 16 and 17 show the photograph of crack growth of some typical elbows. Table 3 shows the crack initiation, TES collapse and maximum loads/moments obtained from the experiments.

Fig. 18 show the load vs. crack mouth opening displacement (CMOD) curves for 400 mm NB elbows.

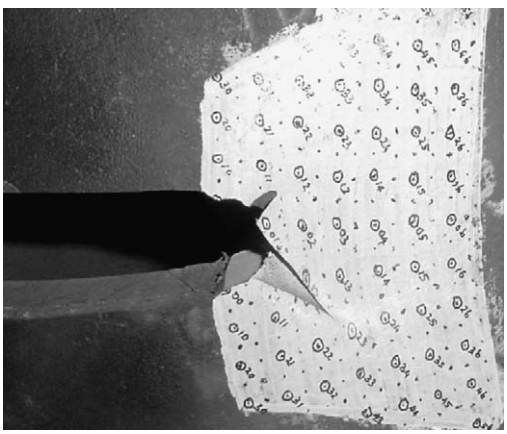

Fig. 16. Crack growth at the end of experiment of 400 mm NB TCC elbow (test no. ELTWEX16-5, $2\theta = 124°$, closing moment).

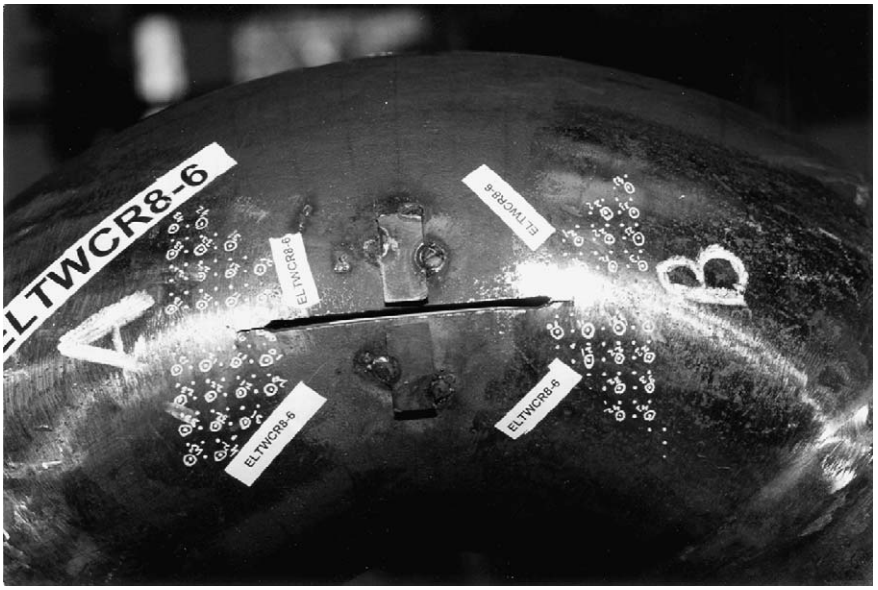

Fig. 17. Crack growth at the end of experiment of 200 mm NB throughwall axially cracked elbow (test no. ELTWCR8-6, $2a = 109$ mm, closing moment). No crack initiation was observed.

Table 3
Experimental crack initiation, TES collapse and maximum loads/moments for elbows

Test ref. no.	Crack initiation		TES collapse		Maximum	
	Load (kN)	Moment[a] (kN m)	Load (kN)	Moment[a] (kN m)	Load (kN)	Moment[a] (kN m)
ELTWIN8-1	112	92.5	119.2	98.4	154	127.2
ELTWIN8-2	92	76	96.9	80	125	103.2
ELTWEX8-4	125	103.2	131.6	108.7	136	112.3
ELTWCR8-6	No initiation		142	117.2	142	117.2
ELTWIN16-1	665.1	558.8	1020	857	1130	949.4
ELTWIN16-2	601.6	505.5	832	699.1	943	792.3
ELTWEX16-3	1360.4	1143	1382	1161.2	1387	1165.4
ELTWEX16-4	995.5	836.4	1173	985.6	1275	1071.3
ELTWEX16-5	742.5	623.9	943	792.3	976	820.1
ELTWCR16-6	No initiation		>Test range		1403[b]	1178.8[b]

[a] Load is converted to moment by multiplying with moment arm length (see Table 2 and Fig. 10).
[b] Test discontinued at almost elastic range.

4. Limit load analysis

The following sections describe the limit load analysis of the test results. All the pipe/elbows are made of carbon steel (ASTM-A333Gr.6) material. However, there are small differences of mechanical properties of 200 and 400 mm NB pipe/elbows materials because of heat-to-heat variation. Elbows are fabricated from same size of pipes and are assumed to have same tensile properties of the parent pipe. Table 4 show the mechanical properties of the 200 and 400 mm NB pipe/elbow materials. The initiation toughness $(J_i)_{SZW}$ is determined as per ESIS (1992).

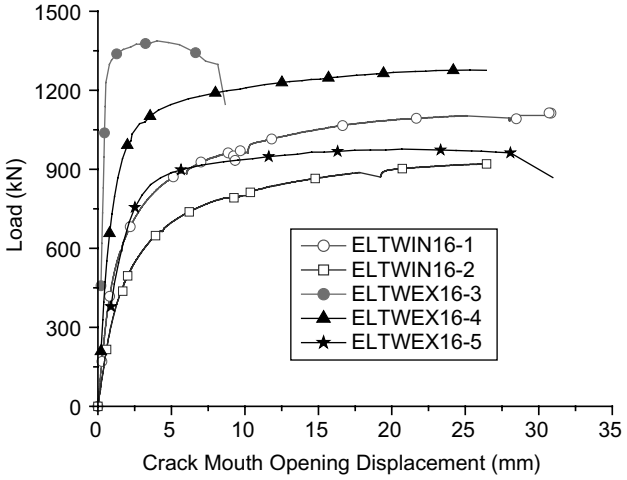

Fig. 18. Experimental load–CMOD curves from 400 mm NB elbows.

Table 4
Mechanical properties of SA 333 Gr 6 steel at room temperature

	200 mm NB pipe/ elbow material	400 mm NB pipe/ elbow material
Yield stress, σ_y (MPa)	288	312
Ultimate tensile stress, σ_u (MPa)	420	459
Young's modulus of elasticity, E (GPa)	203	203
Percentage elongation	36.2	39.1
Percentage reduction in area	76.64	76.15
Poisson's ratio, v	0.3	0.3
Initiation toughness, $(J_i)_{SZW}$ (N/mm)	220	236

4.1. Straight pipe

In this section, the experimental maximum moments are compared with the theoretical limit moments. Limit moment is calculated as follows (Kanninen et al., 1982):

$$M_L = 4R^2 t\sigma_f[\cos(\theta/2) - 0.5\sin(\theta)] \tag{1}$$

where R is the mean radius of the pipe cross section, t is the wall thickness, σ_f is the pipe material flow stress taken as the average of yield and ultimate stress and θ is the semi-crack angle. Moulin and Delliou (1996) suggest a reduction factor of '0.85' to the Eq. (1) to take care of the crack propagation at maximum moment. Eq. (1) is then modified as

$$M_c = 0.85 \times 4R^2 t\sigma_f[\cos(\theta/2) - 0.5\sin(\theta)] \tag{2}$$

Effort has also been made to compare the experimental maximum moment with theoretical predictions of the critical moments as per the 'G factor' approach by Kashima et al. (1990). As per the 'G factor' approach, critical moment of a circumferentially cracked pipe is given as follows:

$$M_c = M_L/G \tag{3}$$

$$G = \{0.692 - 0.0115D_N\} + \{0.188 + 0.0104D_N\}\log_{10}(\theta) \quad 6 \leqslant D_N \leqslant 30 \tag{4}$$

Table 5
Comparison of maximum experimental moments with theoretical predictions (numbers in the bracket show the percentage difference as per Eq. (5))

Test no.	Expt.	Predicted critical moments		
	$\frac{(M_{max})_{expt.}}{4R^2t\sigma_f}$	$\frac{(M_L)_{Eq.\ (1)}}{4R^2t\sigma_f}$	$\frac{(M_c)_{Eq.\ (2)}}{4R^2t\sigma_f}$	$\frac{(M_c)_{Eq.\ (3)}}{4R^2t\sigma_f}$
SPBMTWC8-1	0.6965	0.688 (+1.22)	0.585 (+16.0)	0.681 (+2.22)
SPBMTWC8-2	0.559	0.552 (+1.25)	0.469 (+16.1)	0.524 (+6.26)
SPBMTWC8-3	0.3977	0.405 (−1.83)	0.344 (+13.5)	0.373 (+6.21)
SPBMTWC8-4	0.2702	0.284 (−5.11)	0.241 (+10.8)	0.255 (+5.62)
SPBMTWC16-1	0.4626	0.542 (−17.2)	0.461 (+0.34)	0.491 (−6.13)
SPBMTWC16-2	0.3622	0.406 (−12.1)	0.345 (+4.75)	0.354 (+2.26)
SPBMTWC16-3	0.2468	0.281 (−14.0)	0.239 (+3.04)	0.238 (+3.44)

where D_N is the nominal pipe diameter in inch, θ is the semi-crack angle in degree and M_L is the plastic collapse moment as per Eq. (1). The value of 'G' is more than '1.0' and takes care of the onset of ductile tearing prior to plastic collapse. Table 5 shows the comparison of the experimentally observed maximum moment with the predictions of critical moments as per 'G factor' approach (Eq. (3)), and also the collapse moments (Eq. (1)) and modified collapse moments (Eq. (2)). It also shows the percentage difference between the predicted and experimental values where difference is defined as

$$\% \text{ Difference} = (\text{Experiment} - \text{Predicted}) \times 100/\text{Experiment} \tag{5}$$

Therefore, positive difference indicates that the prediction is conservative. Fig. 19 shows the comparison of experimental maximum moments with the predictions as per Eqs. (1) and (2). It is seen from Table 5 that the critical moments by 'G factor' approach match very closely with the experimental data. However, in one case out of seven, the prediction is slightly non-conservative. It is seen from Table 5 and Fig. 19 that, for 200 mm NB pipes, the collapse moments and experimentally observed maximum moments are very close

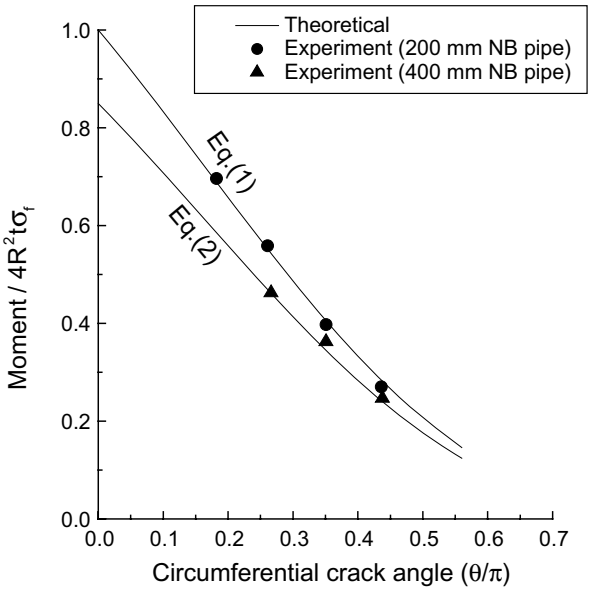

Fig. 19. Comparison of theoretical limit moment with experimental maximum moment.

whereas in case of 400 mm NB pipes, maximum moments are below the collapse moments. This indicates that 200 mm NB pipes have failed in plastic collapse whereas 400 mm NB pipe have failed due to ductile tearing prior to the collapse. This is also corroborated by the load vs. crack growth curves in Fig. 4 where it is seen that before attainment of maximum moment, crack growth in case of 200 mm NB pipes is very small compared to 400 mm NB pipes. Fig. 19 also shows that all the experimental points are conservative with respect to the predictions as per Eq. (2).

4.2. Elbow

Miller (1988) proposed in-plane collapse moment (M_L) equations for throughwall circumferentially cracked (TCC) elbows as follows:

$$\frac{M_L}{M_0} = 1 - \frac{3\theta}{2\pi} \tag{6}$$

$$M_0 = 0.935(4R^2 t\sigma_f)h^{2/3} \tag{7}$$

where 2θ is the circumferential crack angle, $h = tR_b/R^2$ is the elbow factor or bend characteristics, R_b is the mean bend radius, R is the mean radius of elbow cross section, t is the wall thickness and σ_f is the material flow stress usually taken as average of yield and ultimate strength. The equation proposed by Zahoor (1989–1991) for TCC elbow is as follows:

$$M_L = M_0\left[1 - 0.2137\left(\frac{a}{D_m}\right) - 0.0485\left(\frac{a}{D_m}\right)^2 - 1.0559\left(\frac{a}{D_m}\right)^3\right] \tag{8}$$

Applicability : $a/D_m \leqslant 0.8,\ h \leqslant 0.5$ and $D_m/t \geqslant 15$

where M_0 is as defined in Eq. (7), a is the half crack length and D_m is the mean diameter of the elbow cross section. The in-plane collapse moment equation proposed by Zahoor (1989–1991) for throughwall axially cracked short radius elbow is as follows:

$$M_L = M_0\left[1 - 0.15\left(\frac{a}{D_m}\right)\right] \tag{9}$$

However, these equations do not differentiate between opening and closing modes of bending moment. Recently, Chattopadhyay et al. (2004a,b) proposed improved collapse moment formulas for TCC elbows under closing and opening moments which are described briefly in Part 1 of the paper (Chattopadhyay et al., 2005b). These newly proposed equations for closing moments are as follows:

$$M_L = M_0 \cdot X \tag{10}$$

$$M_0 = 1.075h^{2/3}(4R^2 t\sigma_y) \tag{11}$$

The function X is shown in Table 6.

For opening moment, the basic form of the equation is same as closing mode given in Eq. (10) with M_0 and X defined for $5 \leqslant R/t \leqslant 20$ as follows:

$$\frac{M_0}{4R^2 t\sigma_y} = 1.0485h^{1/3} - 0.0617 \tag{12}$$

$$X = 1.127 - 1.8108\left(\frac{\theta}{\pi}\right) \quad \text{for } 45^\circ \leqslant 2\theta \leqslant 150^\circ \tag{13}$$

$$= 1 - 0.8\left(\frac{\theta}{\pi}\right) \quad \text{for } 0^\circ \leqslant 2\theta \leqslant 45^\circ$$

Table 6
Equations of weakening factor (X) for TCC elbows under closing mode (A_0, A_1 and A_2 values for function $X = A_0 + A_1 \cdot (\theta/\pi) + A_2 \cdot (\theta/\pi)^2$)

R/t	A_0	A_1	A_2	θ
5	1.1194	−0.7236	−2.0806	for $45° \leqslant 2\theta \leqslant 150°$ and $X = 1$ for $2\theta < 45°$
7.5	1.1185	−0.3420	−2.5200	for $60° \leqslant 2\theta \leqslant 150°$ and $X = 1$ for $2\theta < 60°$
10	0.9655	1.0152	−4.6800	for $60° \leqslant 2\theta \leqslant 150°$ and $X = 1$ for $2\theta < 60°$
15	1.1400	0.3000	−3.6000	for $90° \leqslant 2\theta \leqslant 150°$ and $X = 1$ for $2\theta < 90°$
20	0.6400	3.4200	−7.9200	for $90° \leqslant 2\theta \leqslant 150°$ and $X = 1$ for $2\theta < 90°$

Table 7
Comparison of experimental collapse moments with theoretical predictions (the bracketed numbers indicate the percentage difference with respect to experimental values)

Test no.	Expt. TES collapse moment (kN m)	Predicted collapse moment (kN m)		
		Chattopadhyay et al. (2004a,b, 2005b), Eqs. (10)–(13)	Miller (1988), Eqs. (6) and (7)	Zahoor (1989–1991), Eqs. (7)–(9)
ELTWIN8-1	98.4	101.1 (−2.7)[a]	82.3 (16.4)	112.8 (−14.6)
ELTWIN8-2	80.0	76.0 (5)	63.6 (20.5)	92.65 (−15.8)
ELTWEX8-4	108.7	100.2 (7.8)	82 (24.6)	113.2 (−4.1)
ELTWEX8-6	117.2	–	–	129.5 (−10.5)
ELTWIN16-1	857.0	847.1 (1.2)	807.9 (5.7)	1109.6 (−29.5)
ELTWIN16-2	699.1	678.8 (2.9)	669.2 (4.3)	971.8 (−39)
ELTWEX16-3	1161.2	1092.3 (5.9)	923.4 (20.5)	1153.6 (0.7)
ELTWEX16-4	985.6	962.1 (2.4)	792.5 (19.6)	1083.3 (−9.9)
ELTWEX16-5	792.3	819.4 (−3.4)	682.8 (13.8)	993.1 (−25.3)
ELTWCR16-6	>Test range	–	–	–

[a] % Difference = [(expt. − predicted)/expt.] × 100%.

The experimental collapse moments evaluated by twice-elastic slope (TES) method are compared with the theoretical predictions through Eqs. (6)–(13). The experimental TES collapse loads are converted to moment by multiplying the load with the moment arm length as given in Table 2 and shown in Fig. 10. Table 7 shows the comparison of collapse moments. It may be seen from Table 7 that the predicted collapse moments using the presently proposed Eqs. (10)–(13) are quite close (with in 8%) to the test data. In contrast, the predictions by Zahoor's (1989–1991) Eqs. (7)–(9) are mostly non-conservative (maximum 39%) and also not close to test data. It may also be noted that Zahoor's equations are not strictly applicable here as these elbows have $R/t \approx 5$ where as Zahoor's equation are valid for $R/t \geqslant 7.5$. This highlights the geometric limitations of the Zahoor's equations. The predictions by Miller's (1988) Eqs. (6) and (7) are seen to be grossly conservative (maximum 25%) with respect to the test data, which was also observed by Yahiaoui et al. (2002).

5. Finite element analysis of test data

This section describes briefly the finite element analysis of the TPB specimens, pipes and elbows for comparison between test results and numerical prediction. More details may be found in Pavankumar et al. (2002, 2003).

5.1. Finite element model

The 3-D elastic–plastic finite element analyses have been carried out on cracked piping components and the specimens. Due to symmetry in both geometry and the loading conditions only one fourth of the TPB specimen, pipe and elbows are modeled. Fine mesh has been provided near the crack front to obtain the steep stress/strain gradients accurately. The side-groove is also modeled in the case of the TPB specimens. Fig. 20 shows the typical finite element mesh for cracked pipe. The finite element mesh for TPB specimen consists of 5606 nodes and 1023 elements, for cracked pipe it is 8231 nodes and 1404 elements and for cracked elbow it is 5763 nodes and 966 elements. The large strain, large displacement relations based on geometry changes are assumed in the analysis. The isoparametric 20-noded elements are adopted in the models. Reduced order of integration ($2 \times 2 \times 2$) is used to eliminate artificial locking under incompressibility condition imposed by plastic deformation. The analyses are done using the finite element program WARP3D (Kopenhoefer et al., 1998). The finite element analysis is done under displacement control to simulate the experimental procedure. Non-linear material behavior is modeled using incremental plasticity with Von Mises yield function associated flow rule and isotropic hardening. The true stress–strain curve obtained from a uni-axial test is given as the input to the material model.

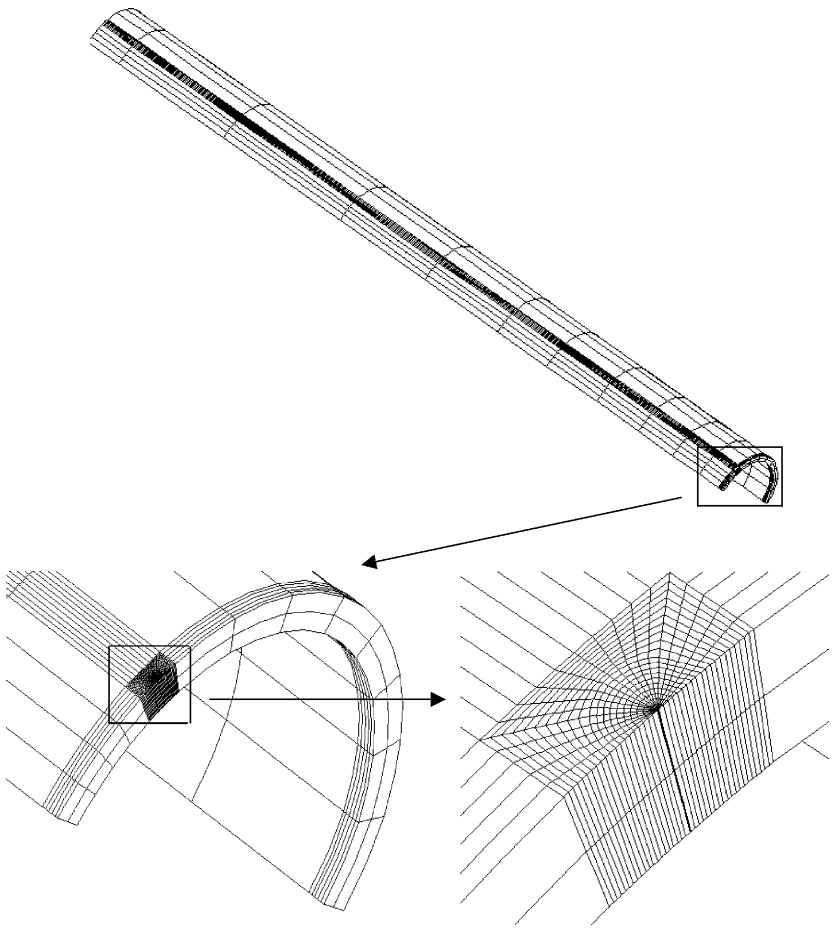

Fig. 20. Finite element mesh employed to model pipe with throughwall circumferential crack.

5.2. Material parameters

The tensile specimens have been machined from 200 mm and 400 NB pipes made of SA333Gr6. Fig. 21 shows the stress–strain curves for 200 mm NB pipe/elbow material. The uni-axial true-stress–strain curve is modeled in piecewise linear fashion as indicated in Fig. 21. The data is given up to the ultimate tensile stress level. After this point, the response is assumed as perfectly plastic. The material with the extended yield plateau, followed by strain hardening region produced numerical instability. Therefore, the yield plateau is replaced as shown in Fig. 21 to eliminate the instability and to allow the use of larger load steps. Solution computed using much smaller load steps and the actual stress–strain curve showed that the results are insensitive to the modification of the stress–strain curve (Pavankumar et al., 2002).

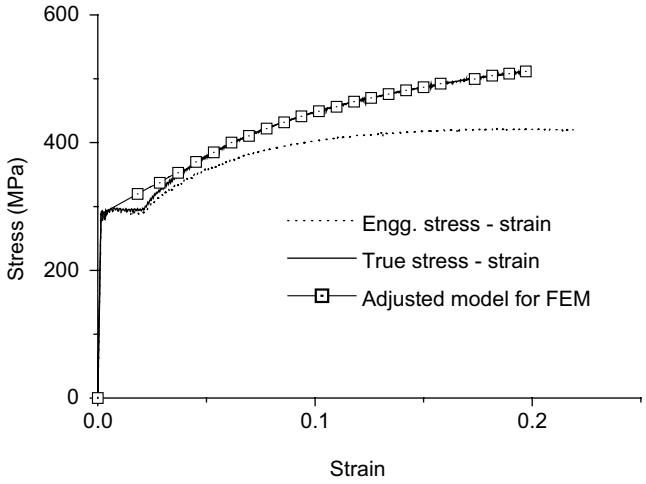

Fig. 21. Stress–strain input to finite element analysis for 200 mm NB pipe/elbow material.

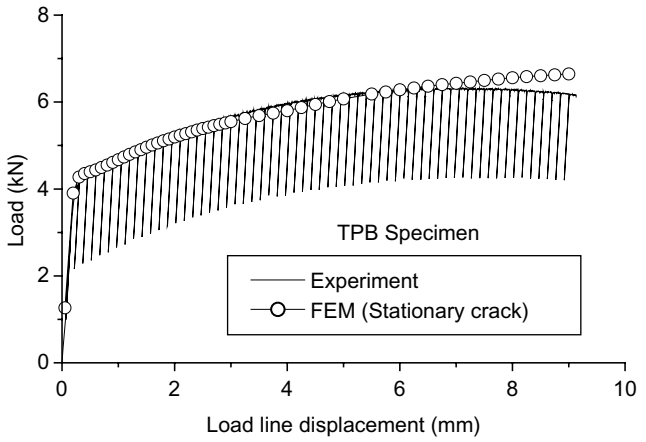

Fig. 22. Comparison of load–deflection curve for TPB specimen.

5.3. Finite element analysis results

5.3.1. Load–deflection curve

The comparison of numerical and experimental load–deflection characteristics of the typical TPB specimen, full-scale pipe and elbow is shown in Figs. 22–24. The numerical and experimental results agreed well. The good matching between experimental and numerical results ensures the validation of the numerical model as well as experimental results. As expected, the numerical model shows higher stiffness just before the maximum load occurs. This is because of the assumption of the stationary crack in the model without considering the crack growth.

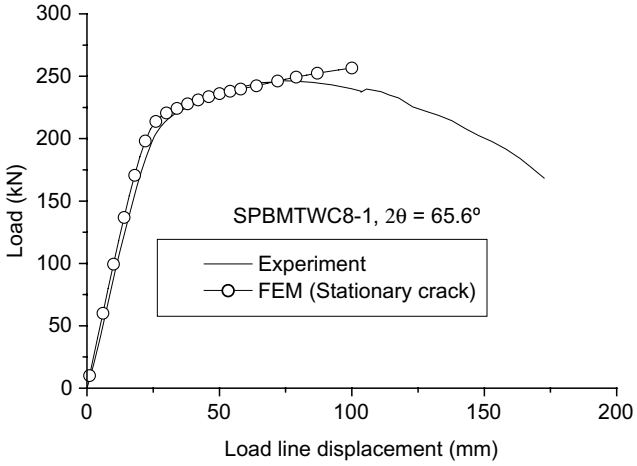

Fig. 23. Comparison of load–deflection curve for one typical tested pipe.

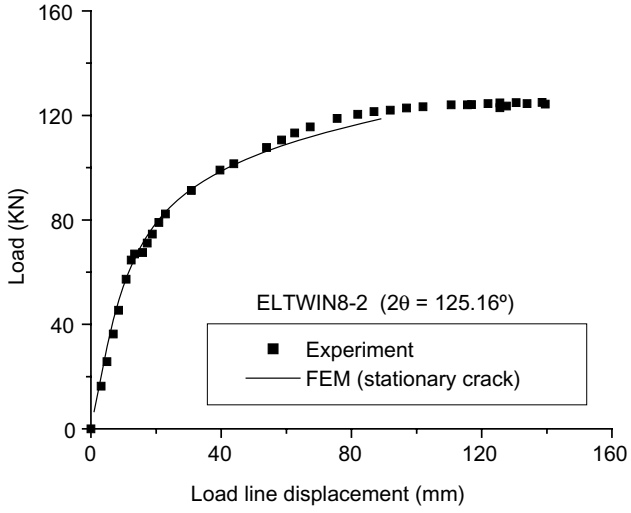

Fig. 24. Comparison of load–deflection curve for one typical tested elbow.

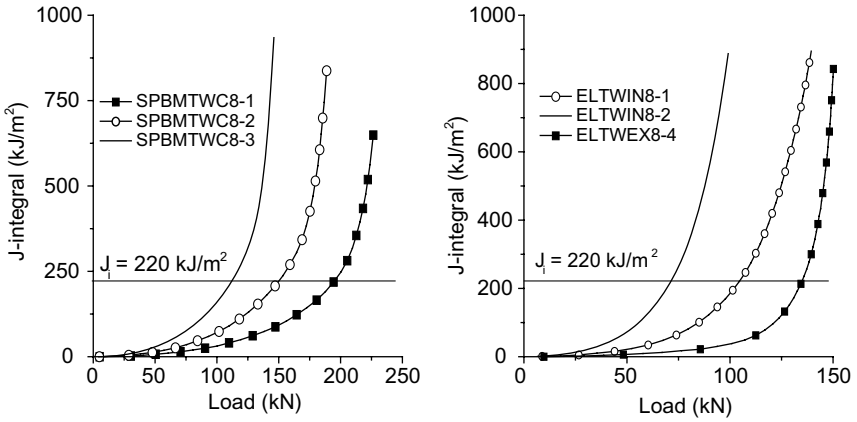

Fig. 25. Determination crack initiation load by finite element analysis for 200 mm NB pipes and elbows.

5.3.2. Comparison of crack initiation load

The initiation toughness $(J_i)_{SZW}$, obtained from the stretched zone width (SZW) can be used to determine the load at onset of ductile crack growth. Investigations (Joyce and Link, 1997; Schuler et al., 1994; Eisele et al., 1994) have shown that $(J_i)_{SZW}$ is more or less independent of stress triaxiality and can be treated as a material property. Hence, it is possible to predict the crack initiation loads by comparing $(J_i)_{SZW}$ determined from the laboratory specimen with the calculated crack driving force (applied J-integral) of the cracked component. The comparison here is shown for 200 mm NB pipes and elbows. The $(J_i)_{SZW}$ for 200 and 400 mm NB pipe/elbow materials is shown in Table 4. Fig. 25 shows the variation of crack driving force (J-integral), obtained from finite element analysis, with the load for 200 mm NB pipes and elbows. It should be noted that the J-integral varies across the thickness. The J-integral is maximum at the mid-thickness and low at the outside/inside surfaces. The average J-integral is calculated using the following equation.

$$J_{ave} = (J_{in} + 4J_{mid} + J_{out})/6.0 \tag{14}$$

This average J-integral is used to predict global crack initiation load. Table 8 compares the experimental and numerical results. As the point of physical crack initiation is difficult to identify experimentally, the

Table 8
Comparison of crack initiation load

Component	Test no.	Crack initiation load (kN)		% Difference (Eq. (5))
		Expt.	Predicted by FEM	
Throughwall cracked pipe	SPBMTWC8-1	194	195	−0.5
	SPBMTWC8-2	148	150	−1.3
	SPBMTWC8-3	116	114	1.7
Throughwall cracked elbow	ELTWIN8-1	112	104	7.1
	ELTWIN8-2	92	70	23.9
	ELTWEX8-4	125	134	−7.2
	ELTWCR8-6	No initiation	–	–
	ELTWIN16-1	665.1	621	6.6
	ELTWIN16-2	601.6	474	21.2
	ELTWEX16-3	1360.4	1249	8.2
	ELTWEX16-4	995.5	989	0.6
	ELTWEX16-5	742.5	770	3.7
	ELTWCR16-6	No initiation	–	–

load at a crack growth of 0.2 mm (SZW ≈ 200 μm for this material (Tarafder et al., 2000)) is considered the crack initiation load. The crack initiation loads predicted by finite element method show good agreement with the experimental results.

6. Transferability of *J–R* curve from specimen to component

Ductile tearing resistance of a material is conventionally characterized by a *J*–resistance (*J–R*) curve, which is obtained from laboratory fracture specimens. The original idea was that one unique fracture resistance curve would suffice to characterize the material. However, testing of different types of specimens under various loading conditions revealed considerable differences in the *J–R* curves, especially in the slopes (Joyce and Link, 1997). This raises the question on transferring the fracture parameters from specimens to the component level. It has been found that constraint/stress triaxiality ahead of crack tip influences the *J–R* curves (Joyce and Link, 1997; Schuler et al., 1994; Eisele et al., 1994). The standards for fracture testing often enforce high-constraint conditions in the specimens to obtain a conservative index of material toughness. The application of *J–R* curves from these specimens to the low-constraint structural applications introduces high degree of conservatism into the design. This can lead to increase in safety margin, when other safety factors are included. The total conservatism inherent in a particular design can become excessively large and the true safety factor is not known. A reverse problem occurs, when the fracture toughness data are obtained on relatively low-constraint specimens and then used in high-constraint applications. This would make the design non-conservative. The transferability of the specimen *J–R* curve to component level is thus an important issue in fracture mechanics. Two-parameter fracture mechanics approach have been tried to describe the effect of constraint on ductile tearing resistance and thereby resolving the issue of transferability. In the two-parameter fracture mechanics approach (Clausmeyer et al., 1991; Betegen and Hancock, 1991; O'Dowd and Shih, 1991; Chao and Ji, 1995; Dodds et al., 1991), the first parameter reflects the scale of crack tip deformation (e.g. *J*-integral) and the second parameter is used to quantify the level of stress triaxiality. If the triaxial conditions are found to be similar then it is believed that the *J–R* curves are transferable within certain circumstances such as the original crack length not influencing the stress triaxiality (Pavankumar et al., 2002). These conditions are evident for the geometries where the ligament length is large for the bending geometries and geometries that are predominately under tension. Joyce and Link (1997) discuss the application of two-parameter fracture mechanics to the analysis of structures.

There are various parameters to quantify the stress triaxiality or constraint ahead of the crack tip. However, in this study, the multi-axiality quotient, '*q*' as proposed by Clausmeyer et al. (1991) and later modified by Pavankumar et al. (2003) is used. The parameters are as defined below:

$$q = \frac{\sigma_e}{\sqrt{3}\sigma_m} \tag{15}$$

where

$$\sigma_m = (\sigma_1 + \sigma_2 + \sigma_3)/3.0 \tag{16}$$

$$\sigma_e = [(\sigma_1 - \sigma_2)^2 + (\sigma_2 - \sigma_3)^2 + (\sigma_3 - \sigma_1)^2]^{1/2}/\sqrt{2} \tag{17}$$

σ_e = von-Mises effective stress; σ_m = hydrostatic stress; σ_1, σ_2, σ_3 are the principal stresses.

The small values of '*q*' represent high degree of stress triaxiality according to this definition. Since, '*q*' varies across the ligament for low-constraint geometries, a question may arise regarding the extent of ligament length to be considered for the comparison of stress triaxiality of specimen and various components. Further, '*q*' alone cannot describe the level of stress triaxiality in a geometry. The slope of '*q*' i.e. dq/dx has

also to be considered along with 'q' to assess the crack growth behavior. Therefore, the triaxiality has to be considered over a certain length in the ligament ahead of the crack tip. Consequently, Pavankumar et al. (2003) modified the 'q' parameter and proposed a new parameter, A_{nq} as defined below:

$$A_{nq} = \frac{\int_{J/\sigma_0}^{5J/\sigma_0} q\,\mathrm{d}x}{\int_{J/\sigma_0}^{5J/\sigma_0} q_c\,\mathrm{d}x} \tag{18}$$

where, q is the multi-axiality quotient, q_c is the critical value of multi-axiality quotient ($= 0.27$), dx is the distance across the ligament, J is the J-integral, σ_0 is the yield stress.

These parameters (i.e. q and A_{nq}) have been evaluated for side-grooved TPB specimen ($a/w = 0.5$) which are machined from 200 mm NB pipes, 200 mm NB pipes having various sizes of throughwall circumferential crack subjected to four point bending load (see Table 1 for details) and also for 200 mm NB elbows having throughwall circumferential cracks at extrados/intrados subjected to closing/opening bending moment (see Table 2 for details). Fig. 26 shows the variation of 'A_{nq}' with J-integral for TPB specimen and pipes and elbows. It may be seen that stress triaxiality ahead of crack tip, quantified by the parameter 'A_{nq}' is almost identical for all these pipes and elbows and TPB specimen. This implies that J–R curves generated from all these components and specimens should be same. Fig. 27 shows the J–R curve generated from TPB specimen, three pipes and three elbows mentioned in Tables 1 and 2. The TPB specimen J–R curve has been extrapolated beyond test range linearly on J–T space keeping the slope same as that at the last test data point as per NUREG Report (1984) where T indicates tearing modulus (Paris et al., 1979). From linearly extrapolated J–T curve, J–R curve has been generated using the equations derived in Chattopadhyay et al. (1999). The J–R curves from pipes are taken from Chattopadhyay et al. (2000). The J–R curves of elbows have been evaluated using the newly proposed η_{pl}' and 'γ' functions (Chattopadhyay et al., 2005b) and details are available in Chattopadhyay et al. (2004c,d). Fig. 27 shows that J–R curve from all these components and specimens are indeed identical, because of identical stress triaxialities in a region ahead of the crack tip. This shows the role of stress triaxialities in the transferability of J–R curve from specimen to component.

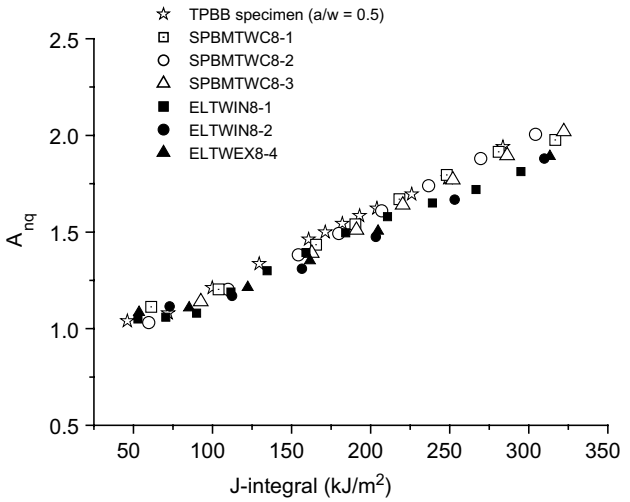

Fig. 26. Variation of constraint parameter (A_{nq}) with J-integral for various pipes and elbows.

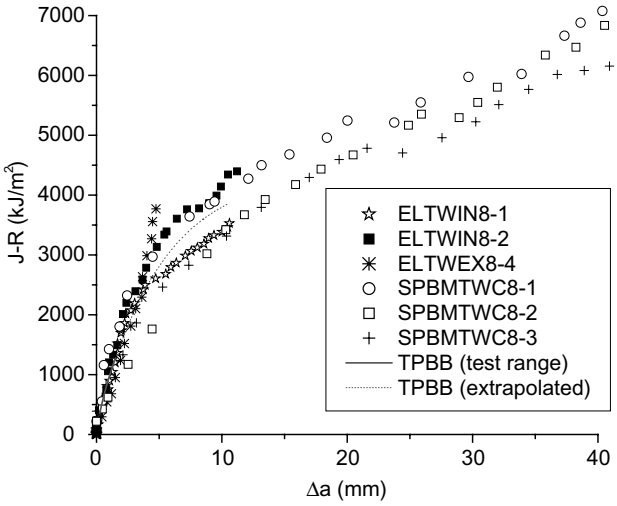

Fig. 27. Comparison of J–R curves from side-grooved TPB specimen and throughwall circumferentially cracked pipes and elbows.

7. Conclusions

Experimental investigations of a comprehensive *Component Integrity Test Program* are described in this paper. As a part of these investigations, fracture mechanics experiments have been conducted on pipes and elbows of 200–400 mm diameter with various crack configurations and sizes under different loading conditions. Tests on small tensile and three point bend specimens, machined from the pipe of same material and heat, have also been done to evaluate the actual stress–strain and fracture resistance properties of pipe/elbow material. The load–deflection curve and crack initiation loads predicted by non-linear finite element analysis matched well with the experimental results. The theoretical collapse moments of throughwall circumferentially cracked elbows, predicted by the recently developed equations, are found to be closer to the test data compared to the other existing equations. The role of stress triaxialities ahead of crack tip is also shown in the transferability of J–resistance curve from specimen to component.

Acknowledgements

The authors acknowledge the contribution of Dr. D.S. Ramachandra Murthy, Mr. P. Gandhi and other staff members of Fatigue Testing Laboratory of Structural Engineering Research Centre (SERC), Chennai, India in conducting the fracture mechanics experiments on pipes and elbows.

References

Betegen, C., Hancock, J.W., 1991. Two parameter characteristics of elastic–plastic crack-tip fields. J. Appl. Mech. 58, 104–110.

Chao, Y.J., Ji, W., 1995. Cleavage fracture quantified by J and A_2. In: Kirk, M., Bakker, A. (Eds.), Constraint Effects in Fracture Theory and Applications, ASTM STP 1244, vol. II. American Society for Testing and Materials, Philadelphia, pp. 3–20.

Chattopadhyay, J., Dutta, B.K., Kushwaha, H.S., 1999. Leak-before-break qualification of primary heat transport piping of 500 MWe Tarapur Atomic Power Plant. Int. J. Press. Vess. Piping 76, 221–243.

Chattopadhyay, J., Dutta, B.K., Kushwaha, H.S., 2000. Experimental and analytical study of three point bend specimen and throughwall circumferentially cracked straight pipe. Int. J. Press. Vess. Piping 77, 455–471.

Chattopadhyay, J., Tomar, A.K.S., Dutta, B.K., Kushwaha, H.S., 2004a. Closed form collapse moment equation of throughwall circumferentially cracked elbows subjected to in-plane bending moment. J. Press. Vess. Technol., ASME Trans. 126, 307–317.

Chattopadhyay, J., Tomar, A.K.S., Dutta, B.K., Kushwaha, H.S., 2004b. Limit load of throughwall cracked elbows: comparison of test results with theoretical predictions. Fatigue Fract. Eng. Mater. Struct. 27, 1091–1103.

Chattopadhyay, J., Dutta, B.K., Kushwaha, H.S., 2004c. New 'η_{pl}' and 'γ' functions to evaluate J–R curves from cracked pipes and elbows: part I—theoretical derivation. Eng. Fract. Mech. 71 (18), 2635–2660.

Chattopadhyay, J., Dutta, B.K., Kushwaha, H.S., 2004d. New 'η_{pl}' and 'γ' functions to evaluate J–R curves from cracked pipes and elbows: part II—experimental and numerical validation. Eng. Fract. Mech. 71 (18), 2661–2675.

Chattopadhyay, J., Pavankumar, T.V., Dutta, B.K., Kushwaha, H.S., 2005a. Fracture experiments on throughwall cracked elbows under in-plane bending moment: test results and theoretical/numerical analyses. Eng. Fract. Mech. 72, 1461–1497.

Chattopadhyay, J., Kushwaha, H.S., Roos, E., 2005b. Some recent developments on integrity assessment of pipes and elbows. Part I: Theoretical investigations. Int. J. Solids Struct., in press, doi:10.1016/j.ijsolstr.2005.06.054.

Clausmeyer, H., Kussmaul, K., Roos, E., 1991. Influence of stress state on the failure behavior of cracked components made of steel. ASME, Appl. Mech. Rev. 44 (2), 77–92.

Darlaston, B.J., Bhandari, S., Franco, C., 1992. Predictions of failure for several of the international pipe tests using the R6 method. In: Int. Conf. Pressure Vessel Tech. Proc., vol. 1: Design Analysis, Paris, May/June.

Dodds, R.H., Anderson, T.L., Kirk, M.T., 1991. A framework to correlate a/W ratio effects on elastic–plastic fracture toughness (J_c). Int. J. Fract. 48, 1–22.

Eisele, U., Herter, K.H., Schuler X., 1994. Influence of the multiaxility of stress state on the ductile fracture behaviour of degraded piping components. In: Schwalbe, K.H., Berger, C. (Eds.), ECF 10, Structural Integrity: Experiments, Models and Applications, vol. 1, pp. 1–10.

ESIS, 1992. ESIS procedure for determining the fracture behavior of materials. ESIS P2-92, European Structural Integrity Society, Appendix 4.

Forster, K., Gruter, L., Setz, W., Bhandari, S., Debaerie, J.P., Faidy, C., Schwalble, K.H., 1996. Crack resistance of austenitic pipes with circumferential through-wall cracks. Int. J. Press. Vess. Piping 65, 335–342.

Greenstreet, W.L., 1978. Experimental study of plastic response of pipe elbows. Report, ORNL/NUREG-24, Oak Ridge National Laboratory, TN.

Griffiths, J.E., 1979. The effect of cracks on the limit load of pipe bends under in-plane bending: experimental study. Int. J. Mech. Sci. 21, 119–130.

Joshi, D.G., Kumar, V., Kar, S., Chadda, V.K., Nigam, R.K., Chattopadhyay, J., Sunil, K.P., Dutta, B.K., Kushwaha, H.S., 1999. Image processing system for fracture experiments of piping components. BARC Internal Report.

Joyce, J.A., Link, R.E., 1997. Application of two parameter elastic–plastic fracture mechanics to analysis of structures. Eng. Fract. Mech. 57, 431–436.

Kanninen, M.F., Zahoor, A., Wilkowski, G.M., Abousayed, I., Marschall, C., Broek, D., Sampath, S., Rhee, H., Ahmad, J., 1982. Instability predictions for circumferentially cracked type 304 stainless steel pipes under dynamic loading. EPRI-NP-2347, vol. 1 and 2. Electric Power Research Institute, Palo Alto, CA.

Kashima, K., Matsubara, M., Miura, N., 1990. Prediction of the failure stress from Japanese carbon Steel pipe fracture experiments. In: Proceedings of the Seminar on Assessment of Fracture Prediction Technology Piping and Pressure Vessels, NUREG/CP-0037, Nashville, Tennessee, pp. 2.22–2.50.

Kopenhoefer, K., Gullerud, A.S., Ruggieri, C., Dodds Jr., R.H., 1998. WARP3D-RELEASE 10.8, Dynamic nonlinear analysis of solids using a preconditioned conjugate gradient software architecture. User's Manual. University of Illinois, Urbana, IL, USA.

Miller, A.G., 1988. Review of limit loads of structures containing defects. Int. J. Press. Vess. Piping 32, 197–327.

Moulin, D., Delliou, P., 1996. French experimental studies of circumferentially through-wall cracked austenitic pipes under static bending. Int. J. Press. Vess. Piping 65, 343–352.

Moulin, D. et al., 1989. Experimental evaluation of J in cracked straight and curved pipes under bending. Tenth International Conference on Structural Mechanics in Reactor Technology, 10th SMiRT, vol. G, pp. 323–326.

NUREG Report of the United States Nuclear Regulatory Commission Piping Review Committee, 1984. Evaluation of potential for pipe breaks. NUREG/CR-1061, vol. 3.

O'Dowd, N.P., Shih, C.F., 1991. Family of crack tip fields characterized by a triaxiality parameter—I: structure of fields. J. Mech. Phys. Solids 39, 898–1015.

Paris, P.C., Tada, H., Zahoor, A., Ernst, H., 1979. The theory of instability of the tearing mode of elastic–plastic crack growth. In: Landes, J.D., Begley, J.A., Clarke, G.A. (Eds.), Elastic–Plastic Fracture, ASTM STP 668. American Society for Testing and Materials, Philadelphia, pp. 5–36.

Pavankumar, T.V., Chattopadhyay, J., Dutta, B.K., Kushwaha, H.S., 2002. Transferability of specimen J–R curve to straight pipe with throughwall circumferential flaw. Int. J. Press. Vess. Piping 79, 127–134.

Pavankumar, T.V., Chattopadhyay, J., Dutta, B.K., Kushwaha, H.S., 2003. Role of stress triaxiality (q) in assessing fracture behavior of cracked components. 29th MPA Seminar, October 9 and 10, MPA, University of Stuttgart, Germany.

Roos, E., Herter, K.-H., Otremba, F., 2000. Testing of pressure vessels, piping, and tubing. In: Mechanical Testing and Evaluation. In: Kuhn, H., Medlin, D. (Eds.), ASM Handbook, vol. 8. American Society of Metals.

Schuler, X., Blind, D., Eisle, U., Herter, K.H., Stoppler, W., 1994. Fracture mechanics evaluation of cracked components with consideration of multiaxiality of stress state. Nucl. Eng. Des. 151, 291–305.

Tarafder, S., Sivaprasad, S., Tarafder, M., Prasad, P., Ranganath, V.R., Swapan Das, 2000. Specimen size and constraint effects on *J–R* curves of SA 333 Gr.6 Steel. Technical report, National Metallurgical Laboratory, Jamshedpur, India.

Wilkowski, G.M. et al., 1989. Degraded piping program—phase II. Summary of technical results and their significance to leak-before-break and in-service flaw acceptance criteria. March 1984–January 1989, NUREG/CR-4082, BMI-2120, vol. 8.

Wilkowski, G.M., Olson, R.J., Scott, P.M., 1998. State-of-the-art report on piping fracture mechanics. NUREG/CR-6540, BMI-2196, United States Nuclear Regulatory Commission.

Yahiaoui, K., Moffat, D.G., Moreton, D.N., 2000. Piping elbows with cracks, part 2: global finite element and experimental plastic loads under opening bending. J. Strain Anal. 35, 47–57.

Yahiaoui, K., Moreton, D.N., Moffat, D.G., 2002. Evaluation of limit load data for cracked pipe bends under opening bending and comparisons with existing solutions. Int. J. Pres. Ves. Piping 79, 27–36.

Zahoor, A., 1989–1991. Ductile Fracture Handbook, vol. 1–3. EPRI-NP-6301-D, N14-1, Research Project 1757-69, Electric Power Research Institute.